Journal of Magnetism and Magnetic Materials 599 (2024) 172103

Contents lists available at ScienceDirect

Journal of Magnetism and Magnetic Materials

journal homepage: www.elsevier.com/locate/jmmm

Research article

Magnetic ground states and hyperfine interactions in $YMnO_3$ using density functional theory

L. Scalise [a,*], A. Mokhles Gerami [b], E. Lora da Silva [c], L.F.D. Pereira [a], A.W. Carbonari [a]

[a] Instituto de Pesquisas Energéticas e Nucleares (IPEN), Av. Professor Lineu Prestes, 2242, 05508-000 São Paulo, SP, Brazil
[b] School of Particles and Accelerators, Institute for Research in Fundamental Sciences (IPM), P.O. Box 19395-5531, Tehran, Iran
[c] IFIMUP, Departamento de Física e Astronomia da Faculdade de Ciências, Universidade do Porto, Rua do Campo Alegre 687, 4169-007 Porto, Portugal

ARTICLE INFO

Keywords:
Multiferroics
Hexagonal manganites
Hyperfine interactions
DFT calculations

ABSTRACT

This study employs the Local Density functional theory (DFT) and the DFT+U extension, to better describe the localized *d*-Mn states, and therefore analyze six magnetic configurations of the Mn ions in hexagonal manganite $YMnO_3$. The respective study was complemented through hyperfine interaction calculations of different atomic configurations. Our focus is on six distinct magnetic configurations, complemented by thorough Hyperfine Interactions (HFI) calculations targeting the most plausible configuration. We find the $P6'_3$ and $P6_3$ configurations are the most probable, aligning with previous research in the field. These configurations also show a strong correlation with experimental observations of magnetic moments, providing new insights into the magnetic ordering of $YMnO_3$. Our results highlight the intricate relationship between magnetic moments and the lattice structure of $YMnO_3$, offering valuable insights into the material's magnetic properties.

1. Introduction

Hexagonal manganite $YMnO_3$ (h-$YMnO_3$), a prominent magnetoelectric material, is renowned for its unique combination of magnetic and ferroelectric properties, particularly at temperatures below approximately 80 K [1,2]. At high temperatures, h-$YMnO_3$ crystallizes at a centrosymmetric structural phase with $P6_3/mmc$ space group, where the Y^{3+} ions are symmetrically positioned at the 2*a* Wyckoff positions. However, as the temperature decreases, these Y^{3+} ions experience asymmetric displacement, meaning they shift from their original, symmetrically aligned locations to new positions that lack this symmetry [3].

This displacement disrupts the centrosymmetry of the crystal, leading to a non-centrosymmetric structure in the P63cm space group (see Fig. 1). Such a structural transition is crucial for the emergence of ferroelectricity, as it enables h-YMnO3 to achieve spontaneous polarization. The displacement of Y^{3+} ions plays a fundamental role in this polarization, leading to an uneven distribution of electrical charges within the crystal lattice. This ionic displacement, together with the hybridization of electronic orbitals – specifically between Yd_{z^2} and O*pz* – significantly contributes to the ferroelectric nature of h-$YMnO_3$ [4]. Additionally, the magnetic properties of the h-$YMnO_3$ stem from the unoccupied *d*-orbitals of the Mn^{3+} ions, which are arranged in a non-collinear manner within the a–b planes, aligned along the *c*-axis. This unique arrangement imparts a complex magnetic profile to the material, including antiferromagnetic characteristics [5,6].

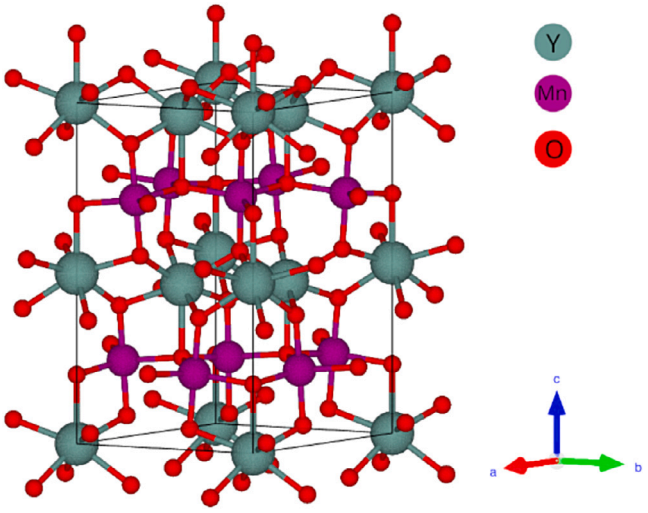

Fig. 1. Crystal Structure of h-$YMnO_3$ in the $P6_3cm$ configuration.

* Corresponding author.
E-mail address: levyscalise@usp.br (L. Scalise).

https://doi.org/10.1016/j.jmmm.2024.172103
Received 26 February 2024; Received in revised form 16 April 2024; Accepted 29 April 2024
Available online 4 May 2024

Recently, $YMnO_3$ has also gained attention as an effective ferroelectric at room temperature, particularly in the non-volatile random-access memory devices [3,7–9]. The strong interaction between its ferroelectric and magnetic properties at low temperatures enhances its multiferroic attributes and thus expands the respective potential for multifunctional and spintronic devices [10]. Other research advancements include the development of $YMnO_3$ ceramics and nanoparticles through low-temperature synthesis, and these show remarkable dielectric and multiferroic properties, which make them highly suitable for practical applications [11,12]. The magnetic structure of h-$YMnO_3$ also positions it as an ideal model for theoretical studies to understand the complexities of multiferroicity in this significant class of materials [3,13].

Despite extensive exploration, the precise magnetic ground state structure of h-$YMnO_3$ remains a contentious topic in the field of materials science. Symmetry-based analyses and experimental data indicate the possibility of six different magnetic configurations, each one with the following spatial groups (see Fig. 2): $P6_3cm$, $P6'_3c'm$, $P6_3c'm'$, $P6'_3cm'$, $P6_3$ and $P6'_3$. Each of these structures is characterized by the angle ϕ between the Mn spin direction and the hexagonal a, b axes [14–17]. In the hexagonal crystal $YMnO_3$, the magnetic space groups significantly influence the spin orientation of the magnetic ions of the material. The $P6_3cm$ and $P6'_3c'm$ space groups confine the orientation of magnetic spins strictly within the hexagonal a–b plane. This restriction means that within these groups, the spins align parallel to the plane formed by the a and b axes of the crystal, without any component along the c-axis. In contrast, the $P6_3c'm'$ and $P6_3$ space groups allow for a phenomenon known as ferromagnetic canting along the c-axis. A small tilt or deviation of the magnetic spins from their primary alignment is referred to as canting. In this case, while the spins primarily lie along the a–b plane, these also evidence a component tilted along the c-axis, all in the same direction, which is a characteristic of ferromagnetic alignment. Conversely, the $P6'_3c'm$ and $P6'_3$ configurations are associated with antiferromagnetic canting. This implies that the spins are slightly canted but in opposite directions, resulting in an antiferromagnetic arrangement. Antiferromagnetic canting introduces additional complexity to the magnetic behavior of the material, exhibiting a more intricate magnetic state [18,19].

The accurate determination of the magnetic ground state configuration of hexagonal $YMnO_3$ is complicated by the symmetric arrangement of Mn ions. This symmetry in the crystal structure can be unknown due to the differences in the spin orientations, making it challenging to distinctly distinguish and characterize the magnetic states. Therefore, understanding the exact magnetic ground state of hexagonal $YMnO_3$ requires accurate theoretical and experimental analysis, taking into account the details of different magnetic space groups and the symmetrical position of Mn ions. In this study, we explore these challenges, aiming to identify the primary magnetic configuration and investigate the possibility of spin canting beyond the a–b planes. Our research employs Density Functional Theory (DFT) calculations for the six proposed configurations by Lima and Lalic [6], coupled with an analysis of hyperfine parameters which is determined through the hyperfine magnetic field. This approach allows us to integrate theoretical findings with existing experimental observations, comprehensively examining the potential ground state configurations of h-$YMnO_3$.

2. Methodology

All calculations were conducted using the all-electron full potential linear augmented plane wave (FP-LAPW) method [20], rooted in the spin-polarized density functional theory (DFT) [21], and implemented using the ELK code [22]. This approach expands electronic wave functions, charge density, and crystal potential into spherical harmonics within atomic spheres around each nucleus and plane waves within the interstitial regions between atoms. The radii of these atomic spheres were set at 2.6 for Y, 2.4 for Mn, and 1.8 for O atoms, measured in atomic units. Inside these spheres, we expanded the partial waves up to $l_{max} = 8$. The plane wave count in the interstitial regions was limited by a cut-off of $K_{max} = 8.0/R_{mt}$, where R_{mt} represents the mean radii of the atomic spheres for Y, Mn, and O. We used a Fourier expansion for the charge density up to $G_{max} = 20$ a.u and a $4 \times 4 \times 2$ k-point grid to sample the irreducible Brillouin-zone for calculations. For considering the exchange and correlation effects, we employed the local spin density approximation (LSDA) [23], which is known to sometimes inaccurately estimate the band gap in semiconductors and insulators. In consideration of both the band gap and the treatment of strongly correlated states within the Mn d-states, we employed the LSDA+U method [24], where the parameter U was systematically varied from 3 eV to 7 eV in steps of 1 eV for the Mn d-bands. The outcome of these simulations identified U = 3 eV as the parameter yielding the lowest total energy, leading to its consistent use throughout the study.

In our study, we incorporated spin–orbit coupling using a second variational method, based on scalar-relativistic eigenfunctions [20]. The total magnetization density was utilized in conjunction with the total charge density and full potential [25]. While we initially set specific orientations for the magnetic moments, these were dynamically adjusted these orientations during the self-consistency cycle to achieve convergence. As a result, the final orientations of the magnetic moments slightly differ from the initial setup.

Along the a–b plane, we initially positioned the magnetic moments of Mn ions at specific phi angles, aligned with the characteristics of each magnetic space group as illustrated in Fig. 2. For the P63 and P6′3 space groups, we maintained a ϕ angle of 10°, as indicated by neutron diffraction studies of [16,26–28]. The z-component of the magnetic moment is expressed in terms of the angle θ, defined as the angle between the moment vector Mn and its respective projection on the a–b plane, which measures the deviation of the Mn moment vector from its projection along the a–b plane.

We ensured that all self-consistent calculations for the various magnetic structures maintained the same precision level. The convergence criterion for these calculations was set to an energy accuracy of 10^{-5} Ha, what means that the error in the difference of energies between two self-consistent cycle must be less than 10^{-5} Ha.

3. Results and discussion

Table 1 presents the key parameters selected for analyzing each structure which are explained in Fig. 2, including the specific angles of Mn spin moments used in our calculations and the values of these properties obtained with and without U parameter. This table also details the outcomes for various critical properties: the intensity of spin moments, the electronic band gap, total energy, and the hyperfine magnetic field (B_{hf}).

From the analysis of the different studied magnetic phases, the P6′3 and P63 structures were found to be energetically the most stable, agreeing partially with findings from Lima et al. [6]. The DFT results revealed minimal variations in the initial angle, suggesting these angles to be crucial for achieving the lowest energy magnetic configuration. For the P63c′m′ and P6′3cm′ configurations, the θ angle consistently remained at zero, indicating a convergence towards the P63 or P6′3 states. Notably, any deviations in these configurations generally tended towards a small ϕ angle of 10.0°, further supporting the results of Lima et al. [6]. However, our computational limitations restricted the exploration of configurations with cantings exceeding $\theta = 6°$. This limitation prevented us from fully investigating whether an initial configuration set at this higher value might eventually converge to a lower energy state. Such an observation highlights the need for more advanced computational resources to fully explore the magnetic behavior of YMnO3 in different configurations, particularly in states with higher canting angles.

In our study, employing only the Local Spin Density Approximation (LSDA), the P6′3 configuration emerged as the lowest energy state. This finding aligns well with previous research performed by Lima et al. [6]

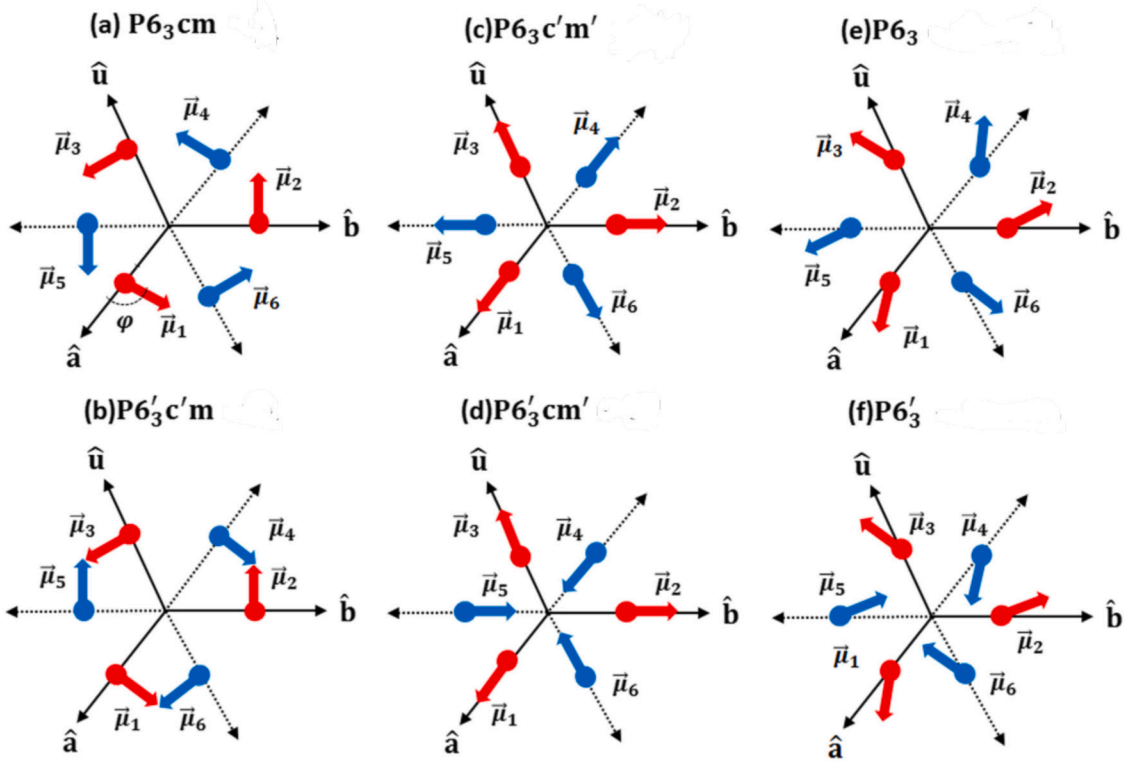

Fig. 2. Representation of possible magnetic structures of the hexagonal $YMnO_3$ compound. Red and blue arrows indicate the Mn spin directions that lie within the adjacent *a–b* planes of the hexagonal unit cell.
Source: Adapted from [6].

Table 1
Angle θ of the spin canting relative to the a–b plane, angle ϕ between the spin magnetic moment of Mn and plane a–b, spin magnetic moment μ_S of the Mn ions, Total Energy (Tot. Ener.) of each configuration, magnetic hyperfine field (B_{hf}^{Mn}) in the Mn site. Each configuration is labeled with the corresponding magnetic spatial group.

	θ		ϕ		μ_S (μ_B/atom)		Tot. Ener. (eV)		B_{hf}^{Mn} (T)	
	LSDA	LSDA+U	LSDA	LSDA+U	LSDA	LSDA+U	LSDA	LSDA+U	LSDA	LSDA+U
P6$_3$cm	0.00	0.00	90.0	90.0	3.44	3.55	−0.4676	−0.7240	49.5	44.6
P6′$_3$c′m	0.00	0.00	90.0	90.0	3.38	3.32	−0.5714	−0.4927	46.1	41.7
P6$_3$c′m′	0.00	0.00	0.00	0.00	3.55	3.40	−0.1523	−0.4098	47.2	42.8
P6′$_3$cm′	0.54	0.96	0.00	0.00	3.51	3.41	−0.1556	−0.5320	48.7	43.2
P6$_3$	5.10	5.14	10.0	10.0	3.07	3.03	−0.1167	−0.9366	44.5	40.9
P6′$_3$	5.06	5.02	10.0	10.0	3.10	2.90	−0.8031	−0.4031	42.6	39.9

and Brown et al. [26]. This specific configuration facilitates an antiferromagnetic alignment along the c-axis. Remarkably, the calculated spin magnetic moment of $\mu S = 3.10\ \mu B$ closely matches the experimentally observed values, which range between 3.14(3) and 3.34(2) μ_B [26]. However, a notable deviation was observed in the band gap estimation. Under LSDA, the band gap was calculated to be 1.21 eV, a value that is lower than the experimentally determined band gap of 1.62 eV [29]. This discrepancy highlights a common limitation of LSDA in accurately predicting band gaps, particularly in semiconductors and insulators, where it often leads to underestimations. This aspect underlines the importance of exploring alternative or more advanced computational methods, such as LSDA+U or hybrid functionals, to achieve more accurate band gap predictions in line with experimental data. By using the LSDA+U method, the magnetic ground state was identified to be P63, which is consistent with the research findings of Brown et al. [26] and Lima et al. [6]. This particular state facilitates ferromagnetic ordering along the *c*-axis. The canting angle θ was calculated to be 5.14°, closely aligning with the initially set parameter. Such a correlation underscores the accuracy of our computational approach in replicating the expected magnetic orientation. The band gap, as calculated by employing LSDA+U, was found to be 1.54 eV. This value is more in line with experimental observations, reflecting the effectiveness of the U parameter in providing a more accurate representation of the band gap. Additionally, the magnetic moment, measured at 3.03 μB, closely mirrors the expected value, demonstrating a minor deviation from the results obtained through the LSDA method.

Although Fe and Mn are different atoms, both are 3d magnetic atoms and can present different valences. Nevertheless, the number of 3d unpaired electrons for both atoms can be the same, depending on the valence. Doping $YMnO_3$ with small concentration of Fe can, of course, disturb local fields, however, we are not expecting an extreme difference in the hyperfine field for Fe-doped and undoped $YMnO_3$. By using Mossbauer spectroscopy at ^{57}Fe nuclei embedded in the material through doping with iron atoms at a concentration of around 5%, the experimental B_{hf} on hexagonal $YMnO_3$ has been studied [30]. The lowest temperature observations (11–12 K) yielded four fraction sites, whose values of B_{hf} ranged from 40.0 T to 44.4 T, all with an angle of 90° between the magnetization and the EFG z axis [30]. Of course, the Fe atom is not the same as the Mn atom, but they both have an incomplete 3d shell and +3 valence in $YMnO_3$ (Mn may have a percentage of +4 valence). The primary distinction between Fe and Mn is the contribution from the probe atom itself as a result of this

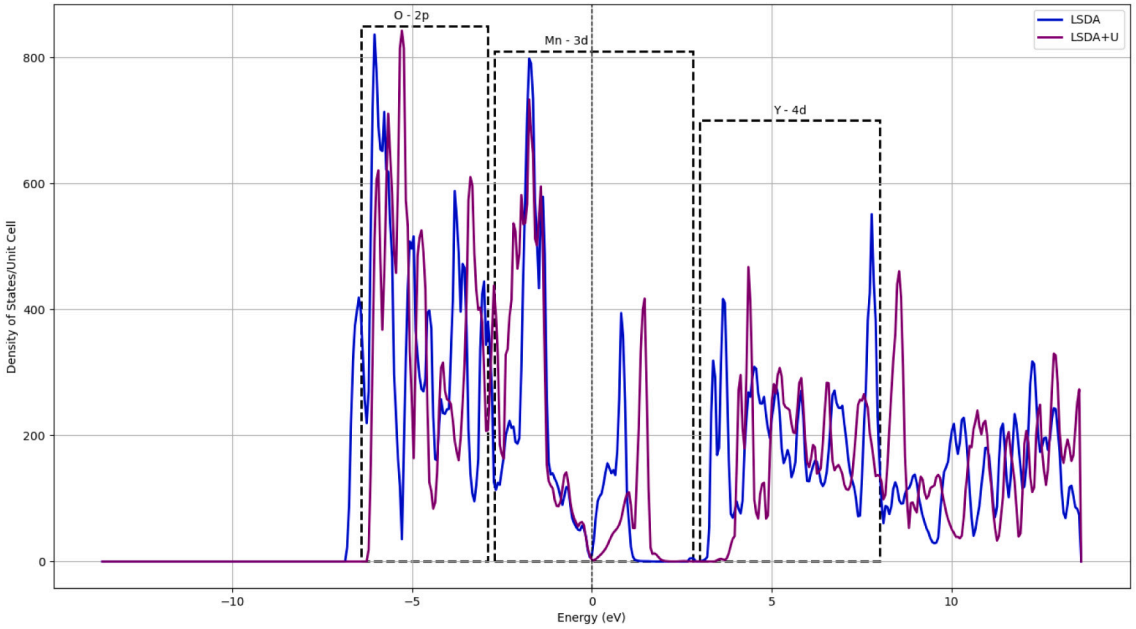

Fig. 3. Total electronic density of states (TDOS) of the lowest-energy spin configurations $P6_3$ in YMnO3, calculated by LSDA approach.
Source: The Authors.

difference in the number of unpaired 3d electrons, which is one more than the Mn atom has. This difference would only be accountable for the core polarization effect at the nucleus. The contribution from the nearest Mn atoms is the same for Mn or Fe probes since distances and the electronic configuration of the neighborhood are not affected by the probes. This difference would only be relevant to the core polarization effect at the nucleus. Since the probes do not affect neighborhood distances or electronic configuration, the contribution from the nearest Mn atoms is the same for Mn or Fe probes.

The LSDA+U calculations for the hexagonal ($P6_3cm$) $YMnO_3$ yielded findings for B_{hf} = 44.6 T. Regardless of the difference between Mn and Fe, already pointed out above, this number falls within the range of experimental values obtained at ^{57}Fe in Fe-doped $YMnO_3$ using Mossbauer spectroscopy.

The evaluation of hyperfine parameters in our study was constrained by the limited availability of comparative data in the existing literature. Despite this, our calculations using both LSDA and LSDA+U methods provided valuable insights. We observed that these computational approaches did not significantly alter the HFI values, Notably, the planarity of this landscape tends to lead to convergence within local minima during computational processes. Such a characteristic can significantly influence the outcomes of our calculations, especially regarding the determination of hyperfine parameters. This aspect of hexagonal RMnO3 necessitates careful consideration in computational modeling to ensure accurate predictions of its magnetic and electronic properties.

It is essential to acknowledge that DFT has limitations, given the approximations of exchange and correlation effects and technical errors. Considering these aspects, the P63 or P6′3 configurations emerge with more emphasis as the magnetic ground state of h-$YMnO_3$. The Mn spin moments' canting along the c-axis, influenced by Dzyaloshinskii-Moriya interactions [3,31] and single-ion anisotropy [32], should be captured in spin–orbit coupling. This inclination is also shaped by the super-exchange interaction of Mn–O–Mn, favoring the permanence of Mn in the a–b plane.

Fig. 3 presents the total density of electronic states (TDOS) for the lowest energy manganese (Mn) spin configuration for hexagonal $YMnO_3$. This electronic structure aligns well with the findings of Lima et al. [6]. Employing both the Local Density Approximation (LSDA) and the LSDA+U (where U is the Hubbard correction) methods, we observed the material to be insulating, evidenced by the presence of a non-zero band gap. Notably, the LSDA+U approach, while maintaining the insulating character, alters the band gap significantly. It achieves this by segregating the occupied Mn states from the unoccupied 3d states. This separation has a consequential impact on the magnetic moments of the Mn ions, reflecting the sensitivity of Mn spin moments to p-d hybridization variations across different magnetic configurations. This result, illustrated in Table 1, highlights the importance of considering electronic structure modifications in understanding the magnetic properties of such complex materials. The LSDA+U method, with its adjustment of the band gap and Mn states, offers a deeper and more detailed insight into the electronic and magnetic characteristics of hexagonal $YMnO_3$, which is essential for accurate theoretical predictions and potential material applications.

4. Conclusions

In this study, we employed density functional theory (DFT) to analyze the six potential non-collinear magnetic structures of hexagonal $YMnO_3$ in its ferroelectric phase, utilizing the full-potential linear augmented plane wave (FP-LAPW) method with the ELK code. We incorporated exchange and correlation effects through LSDA and LSDA+U approximations and included spin–orbit coupling. Our analysis focused on computing the total energies for each magnetic configuration and exploring the feasibility of canting in the Mn ion magnetic moments along the c-axis, as well as investigating hyperfine parameters associated with these ions.

Our results indicate that the P63 and P6′3 configurations are the most likely candidates for the magnetic ground state of h-$YMnO_3$. However, experimental verification remains a challenge due to the minimal energy differences between these configurations. Both configurations suggest the presence of canting in Mn moments, potentially leading to weak ferromagnetism in P63 and weak antiferromagnetism in P6′3 along the c-axis. Future studies should aim to validate these indications.

This research enhances our understanding of the magnetic properties of h-YMnO3, highlighting the complexity of its interactions and the need for sophisticated theoretical approaches for in-depth analysis. The emergence of P63 and P6′3 configurations as the leading candidates for the ground state paves the way for further investigations to elucidate the full magnetic behavior of this important class of materials.

CRediT authorship contribution statement

L. Scalise: Writing – review & editing, Writing – original draft, Visualization, Validation, Software, Project administration, Methodology, Investigation, Formal analysis, Data curation, Conceptualization. **A. Mokhles Gerami:** Writing – review & editing, Visualization, Validation, Resources, Methodology, Investigation, Formal analysis, Data curation, Conceptualization. **E. Lora da Silva:** Writing – review & editing, Visualization, Validation, Software, Resources, Methodology, Investigation, Formal analysis, Data curation,. **L.F.D. Pereira:** Visualization, Validation, Formal analysis, Supervision,. **A.W. Carbonari:** Writing – review & editing, Visualization, Validation, Supervision, Resources, Project administration, Methodology, Investigation, Formal analysis, Funding acquisition, Conceptualization.

Declaration of competing interest

The authors declare that they have no known competing financial interests or personal relationships that could have appeared to influence the work reported in this paper.

Data availability

Data will be made available on request.

Acknowledgments

The authors acknowledge the CNPq and CAPES (Brazilian funding agencies) for financial help.

References

[1] Saurabh Ghosh, Hena Das, Craig J. Fennie, Linear magnetoelectricity at room temperature in perovskite superlattices by design, Phys. Rev. B 92 (18) (2015) 184112.
[2] Ali Mohamed Gebrel Zohra, Synthesis and magnetic properties of pure and substituted yttrium cuprates and manganites, University of Belgrade, PhD Thesis (2013).
[3] Bas B. Van Aken, Thomas T.M. Palstra, Alessio Filippetti, Nicola A. Spaldin, The origin of ferroelectricity in magnetoelectric YMnO3, Nat. Mater. 3 (3) (2004) 164–170.
[4] Jens Kreisel, Michel Kenzelmann, Multiferroics-the challenge of coupling magnetism and ferroelectricity, Europhys. News 40 (5) (2009) 17–20.
[5] D.G. Tomuta, S. Ramakrishnan, G.J. Nieuwenhuys, J.A. Mydosh, The magnetic susceptibility, specific heat and dielectric constant of hexagonal YMnO3, LuMnO3 and ScMnO3, J. Phys.: Condens. Matter 13 (20) (2001) 4543.
[6] A.F. Lima, M.V. Lalic, Ground-state magnetic structure of hexagonal YMnO3 compound: A non-collinear spin density functional theory study, J. Magn. Magn. Mater. 416 (2016) 236–240.
[7] Sandra H. Skjærvø, Quintin N. Meier, Mikhail Feygenson, Nicola A. Spaldin, Simon J.L. Billinge, Emil S. Bozin, Sverre M. Selbach, Unconventional continuous structural disorder at the order-disorder phase transition in the hexagonal manganites, Phys. Rev. X 9 (3) (2019) 031001.
[8] Wilfrid Prellier, M.P. Singh, Pattukkannu Murugavel, The single-phase multiferroic oxides: from bulk to thin film, J. Phys.: Condens. Matter 17 (30) (2005) R803.
[9] Rehana P. Ummer, Nandakumar Kalarikkal, Multiferroic polymer film composites for memory application, in: Chemical Technology and Informatics in Chemistry with Applications, CRC Press, 2019, pp. 175–194.
[10] Indu Sharma, Renu, A. Pananjay Tiwari, A review on multiferroic in magnetic field sensor applications, Int. J. Basic Appl. Sci. 11 (2022) 37–48.
[11] Meng Wang, Ting Wang, Shenhua Song, Muchakayala Ravi, Renchen Liu, Shishan Ji, Enhanced multiferroic properties of YMnO3 ceramics fabricated by spark plasma sintering along with low-temperature solid-state reaction, Materials 10 (5) (2017) 474.
[12] Tokeer Ahmad, Irfan H. Lone, Mohd Ubaidullah, Structural characterization and multiferroic properties of hexagonal nano-sized YMnO 3 developed by a low temperature precursor route, RSC Adv. 5 (71) (2015) 58065–58071.
[13] L.W. Martin, S.P. Crane, Y.H. Chu, M.B. Holcomb, M. Gajek, Mark Huijben, Chan-Ho Yang, N. Balke, R. Ramesh, Multiferroics and magnetoelectrics: thin films and nanostructures, J. Phys.: Condens. Matter 20 (43) (2008) 434220.
[14] S.L. Holm, A. Kreisel, T.K. Schäffer, A. Bakke, M. Bertelsen, U.B. Hansen, M. Retuerto, Jacob Larsen, D. Prabhakaran, P.P. Deen, et al., Magnetic ground state and magnon-phonon interaction in multiferroic h- YMnO 3, Phys. Rev. B 97 (13) (2018) 134304.
[15] Kiran Singh, Marie-Bernadette Lepetit, Charles Simon, Natalia Bellido, Stéphane Pailhès, Julien Varignon, Albin De Muer, Analysis of the multiferroicity in the hexagonal manganite YMnO3, J. Phys.: Condens. Matter 25 (41) (2013) 416002.
[16] Tapan Chatterji, Neutron scattering investigations of multiferroic YMnO 3, Pramana 71 (2008) 847–858.
[17] Tara N. Tošić, Quintin N. Meier, Nicola A. Spaldin, Influence of the triangular Mn-O breathing mode on magnetic ordering in multiferroic hexagonal manganites, Phys. Rev. Res. 4 (3) (2022) 033204.
[18] Miguel Algueró, J.A. Quintana-Cilleruelo, O. Peña, Alicia Castro, Magnetic properties across the YMnO3-BiFeO3 system designed for phase-change magnetoelectric response, Mater. Sci. Eng. B 266 (2021) 115055.
[19] M. Ramakrishnan, Y. Joly, Q.N. Meier, M. Fechner, M. Porer, S. Parchenko, Y.W. Windsor, E.M. Bothschafter, F. Lichtenberg, U. Staub, Antiferromagnetic spin canting and magnetoelectric multipoles in h- YMnO 3, Phys. Rev. Res. 5 (1) (2023) 013203.
[20] David Singh, Lars Nordström, Planewaves, Pseudopotentials and the LAPW Method, second ed., 2005.
[21] Rudolf Zeller, Spin-polarized dft calculations and magnetism, in: Computational Nanoscience: Do It Yourself, Vol. 31, Citeseer, 2006, pp. 419–445.
[22] The Elk Code. http://elk.sourceforge.net/.
[23] John P. Perdew, Yue Wang, Accurate and simple analytic representation of the electron-gas correlation energy, Phys. Rev. B 45 (1992) 13244–13249.
[24] Vladimir I. Anisimov, F. Aryasetiawan, A.I. Lichtenstein, First-principles calculations of the electronic structure and spectra of strongly correlated systems: the LDA+ U method, J. Phys.: Condens. Matter 9 (4) (1997) 767.
[25] Lars Nordström, David J. Singh, Noncollinear intra-atomic magnetism, Phys. Rev. Lett. 76 (1996) 4420–4423.
[26] P.J. Brown, T. Chatterji, Neutron diffraction and polarimetric study of the magnetic and crystal structures of HoMnO3 and YMnO3, J. Phys.: Condens. Matter 18 (44) (2006) 10085.
[27] I. Gélard, C. Dubourdieu, S. Pailhès, S. Petit, Ch. Simon, Neutron diffraction study of hexagonal manganite YMnO3, HoMnO3, and ErMnO3 epitaxial films, Appl. Phys. Lett. 92 (23) (2008).
[28] Andrew J. Overton, James L. Best, Ian Saratovsky, Michael A. Hayward, Influence of topotactic reduction on the structure and magnetism of the multiferroic YMnO3, Chem. Mater. 21 (20) (2009) 4940–4948.
[29] Rüdiger Schmidt-Grund, Steffen Richter, Stefan G. Ebbinghaus, Michael Lorenz, Carsten Bundesmann, Marius Grundmann, Electronic transitions and dielectric function tensor of a YMnO3 single crystal in the NIR-VUV spectral range, RSC Adv. 4 (2014) 33549–33554.
[30] D. Karoblis, A. Zarkov, E. Garskaite, K. Mazeika, D. Baltrunas, G. Niaura, A. Beganskiene, A. Kareiva, Study of gadolinium substitution effects in hexagonal yttrium manganite $YMnO_3$, Sci. Rep. 11 (2021) 2875.
[31] Arpita Paul, Priya Sharma, Umesh V. Waghmare, Spin-orbit interaction, spin-phonon coupling, and anisotropy in the giant magnetoelastic effect in YMnO 3, Phys. Rev. B 92 (5) (2015) 054106.
[32] I.V. Solovyev, M.V. Valentyuk, V.V. Mazurenko, Magnetic structure of hexagonal YMnO 3 and LuMnO 3 from a microscopic point of view, Phys. Rev. B 86 (5) (2012) 054407.